Model Structures for MCM-41 Materials: A Molecular Dynamics Simulation

B. P. Feuston* and J. B. Higgins

Mobil Research and Development Corporation, Central Research Laboratory, Princeton, New Jersey 08543

*Received: December 3, 1993; In Final Form: February 16, 1994**

Model structures for MCM-41 materials have been obtained using the classical molecular dynamics simulation technique with effective interaction potentials. A series of MCM-41 models with various lattice constants and wall thicknesses have been generated and analyzed. The density of T-sites, concentration of silanols, distribution of ring sizes, and the X-ray diffraction patterns were calculated for each structure with the latter compared to the experimental results. The results indicate (i) the calculated X-ray diffraction pattern of the ≥10 Å wall amorphous silica models are in excellent agreement with those observed experimentally, (ii) structures with wall thicknesses less than 7 Å are most likely unstable and give rise to X-ray diffraction patterns inconsistent with experiment, (iii) structures formed with smaller micelle templates require thicker walls to achieve thermodynamic stability, and (iv) models whose calculated X-ray diffraction patterns are consistent with observed patterns have 17–28% of the silicon as silanols, in good agreement with the 8–27% reported from NMR.

Introduction

A generally accepted structural model for MCM-41 materials consists of a hexagonal arrangement of cylindrical pores embedded in a matrix of amorphous silica.[1,2] Though the hexagonal cell parameter may be accurately determined from the X-ray diffraction pattern, the diameter of the cylindrical pores and the wall thickness are inferred from the micelle template and from physisorption experiments. To better understand the structure and in particular the relationship between pore size and the wall thickness, a molecular dynamics (MD) simulation has been performed.

While experiments may accurately measure average structure and particle dynamics, MD simulations provide an atomic level description of the atomistic motion and microstructure that give rise to the observed properties.[3] State-of-the-art techniques can now calculate the properties of nearly 100 atoms and several hundred electrons directly from first principles, i.e., solutions to Schrödinger's equation. Unfortunately, these quantum molecular dynamics simulations (QMD) still require the services of the fastest supercomputers. However, many systems may be adequately described using the classical molecular dynamics (CMD) approach, where simulations of 10^3–10^4 atoms are routinely performed on computer workstations. This latter approach is sufficient for an initial description of the structure and dynamics of MCM-41 materials.

In the CMD method, the full quantum mechanical description (Schrödinger's equation) is approximated by Newton's equation of motion,

$$\vec{F}_i = m\vec{a}_i \tag{1}$$

with

$$\vec{F}_i = -\vec{\nabla} V(\{\mathbf{r}_j\}) \tag{2}$$

where V is an effective interaction potential and $\{\mathbf{r}_j\}$ are the atomic position vectors for $1 \le j \le N$, N being the total number of atoms. The adjustable parameters in this effective potential are usually fitted using the available empirical data (e.g., bond lengths and angles, elastic constants, bulk moduli, etc.) for the system being investigated. Given a interaction potential and an initial configuration, the system is allowed to evolve according to eqs 1 and 2. The fifth-order Gear's algorithm has been used to integrate the $3N$ equations of motions (eq 1).[4] The temperature of the system is calculated directly from the total kinetic energy. By scaling the atomic velocities, the temperature of the system may be changed as needed. By heating the atoms and allowing the system to achieve thermal equilibrium, much of the $3N$-dimensional configuration space can be sampled. Subsequent cooling will localize the atoms in regions of low potential energy (binding sites) as determined by the effective potential. Such heating and cooling is analogous to annealing the system.

In the present approach, a 3-dimensional hexagonal array of cylindrical pores is formed with silicon and oxygen inserted in the space available between the pores. While the atoms making up the template are frozen in place, the silicon and oxygen atoms are allowed to move under the forces derived from the effective interaction potential. A relaxed structure is obtained by heating the system (i.e., increasing the kinetic energy) and allowing the Si and O atoms to overcome local energy barriers. A deep local minimum, associated with an amorphous structure, is achieved when the energy cannot be significantly lowered on the time scale of the simulation (~50 ns). Note that crystallization of zeolite frameworks, characterized by a global minimum, requires on the order of minutes to hours to occur in the laboratory. Clearly, the MD results are very sensitive to the choice of the interatomic potential. Therefore, as in all MD simulations, it is important that the effective interaction potential reflect as best as possible the chemistry and physics of the system under investigation.

Effective Interaction Potential

The cohesive energy of N interacting atom can be described by a potential energy function of the atomic positions,

$$V(\mathbf{r}_1,\mathbf{r}_2,\ldots,\mathbf{r}_N) = \sum_{i<j} V_2(|\mathbf{r}_i-\mathbf{r}_j|) + \sum_{i<j<k} V_3(\mathbf{r}_i,\mathbf{r}_j,\mathbf{r}_k) + \ldots + V_N(\mathbf{r}_1,\mathbf{r}_2,\ldots,\mathbf{r}_N) \tag{3}$$

where V_n represents a n-body potential. For the above expansion to be reasonable, the dominant potential energy contribution will come from pair interactions V_2, while the n-body term will be less than the $(n-1)$-body term, for $3 < n < N$. In some cases such as ionic (alkali halides) and van der Waals (inert gases) systems, two-body potentials alone have been found to be sufficient. But pair potentials which neglect V_3 and higher-order terms are inadequate for properly describing systems which exhibit covalent bonding, thereby requiring the inclusion of a directional-dependent term in the effective interaction potential. An empirical interaction potential for vitreous silica (v-SiO_2) has been previously

* Abstract published in *Advance ACS Abstracts*, April 1, 1994.

0022-3654/94/2098-4459$04.50/0

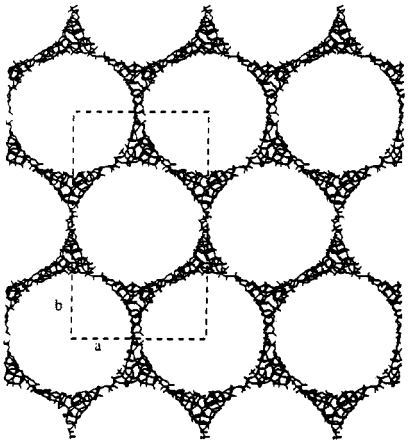

Figure 1. Model for MCM-41 with lattice constant a = 44.6 Å and a wall thickness of 5.9 Å. The unit cell for the molecular dynamics simulation is indicated by the dotted line. The MD cell length along the c direction is 10.0 Å.

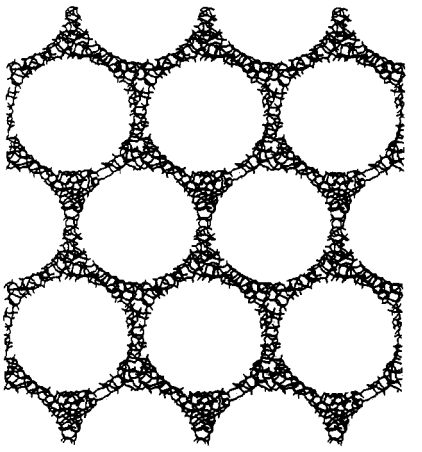

Figure 2. Model for MCM-41 with lattice constant of 44.6 Å and a wall thickness of 8.4 Å.

developed to account for the tetrahedral bonding configuration in silica and silicate glasses.[5] The potential has been successfully employed in simulations of bulk v-SiO_2, sodium trisilicate glasses, silica surfaces, and silica surface-water interactions as well as in the study of polymerization in silicic acid sols.[5-9]

The two-body contribution to the potential has two terms,

$$V_2(\mathbf{r}_{ij}) = A_{ij}\frac{\exp\left(\frac{-\mathbf{r}_{ij}}{\rho}\right)}{\mathbf{r}_{ij}} + Z_iZ_j\frac{\operatorname{erfc}\left(\frac{\mathbf{r}_{ij}}{\beta_{ij}}\right)}{\mathbf{r}_{ij}} \qquad (4)$$

where the first term has the form of a Born–Mayer–Huggins short-range repulsion while the second term is a truncated Coulomb potential with $\{Z_i\}$ as the formal charges, −2 and +4 for O and Si, respectively. All the interaction-dependent parameters in eq 4 (A_{Si-Si}, A_{Si-O}, A_{O-O}, ρ, β_{Si-Si}, β_{Si-O}, β_{O-O}) were fitted to the observed bond lengths, structure factor, and phonon spectrum of bulk silica. The three-body term penalizes the energy whenever the bond angles differ from the preferred tetrahedral angle (θ_0).

$$V_3(\mathbf{r}_{ij},\mathbf{r}_{ik},\theta_{jik}) = \lambda_i \exp\left(\frac{\gamma_{ij}}{\mathbf{r}_{ij}-\mathbf{r}_c} + \frac{\gamma_{ik}}{\mathbf{r}_{ik}-\mathbf{r}_c}\right)(\cos\theta_{jik} - \cos\theta_0)^2 \qquad (5)$$

This form of three-body potential has continuous derivatives with $\mathbf{r}_c$ and γ_{ij} chosen so that this contribution to the total energy goes smoothly to zero beyond the first-neighbor distances. A detailed discussion of this potential along with a complete list of parameters is given in ref 5.

Modeling MCM-41

Molecular dynamics simulations were performed on pseudohexagonal orthorhombic cells with periodic boundary conditions. Each cell contains two parallel micelles (pores) packed in a hexagonal arrangement with *P6mm* symmetry. This packing geometry is equivalent to the C-centered orthorhombic cells illustrated in Figure 1 with $a\sqrt{3} = b$. The repeat distance for the c axis in all the models was set around 10 Å. The micelles were constructed by rings of Lennard-Jones (LJ) atoms, close-packed to form a cylinder. Atoms forming the micelle were frozen throughout the simulations. The silicate framework atoms surrounding the micelles have only P1 symmetry. The interaction between the LJ atoms and silica is best characterized as a hard wall interaction with a small positive wall charge to ensure an oxygen-terminated surface. Because of the periodic boundary conditions (i.e., translational symmetry), the silicate framework is not truly amorphous. This feature is not significant with respect to the MD simulation since the cell repeat distance is much larger than the interatomic distances; however, it must be considered in the interpretation of the calculated diffraction patterns discussed below. A preferred model with a truly amorphous framework consists of a much larger cell with cell parameters of several thousand angstroms and no periodic boundary conditions. The practical limitation to the use of larger cells is the tremendous increase in computer time necessary to run the MD simulations and the diffraction calculations.

Six models for MCM-41 have been investigated. In the first three, the diameter of the micelles was kept constant (39.6 Å) while the wall thickness varied at 5.3, 7.7, and 13.0 Å. In the final three structures, the hexagonal micelle (pore) spacing was held constant at 44.6 Å while the wall thickness varied at 5.9, 8.4, and 10.9 Å. The 44.6-Å cell constant was chosen for the latter three models to facilitate comparison with previously published experimental results.[1]

After the micelles were placed in the MD cell, two different approaches were used to insert the silica. In the first approach, Si atoms were randomly inserted between the cylinders with a density close to that of v-SiO_2, being careful not to place any two Si atoms within 2.5 Å of each other. Oxygen atoms were then placed between all neighboring pairs of Si atoms. Cylindrical sheets of SiO_2 similar to the carbon fullerene straws were placed around the micelle in the second approach. In this way the SiO_2 is ordered about the micelle and disordered in the regions of overlap. In both approaches, the initial structures were allowed to relax using the effective three-body potential and the MD simulation technique. The structures were heated to 900 K and allowed to reach thermal equilibrium before cooling to room temperature. In addition, atoms were removed or inserted as needed to achieve a uniform stoichiometry with nearly all the silicon atoms bonded to four oxygens. This combined procedure of annealing and manual atom placement was repeated until all the necessary bonds were formed and the total energy of the system could no longer be reduced. Subsequent analysis showed that memory of the starting configuration was not retained in these final structures. The total number of silicon and oxygen atoms in the final structural models ranged from 764 to 1936.

The fully-relaxed structures provide a good model for the formation of a silica glass around ideal cylindrical micelles. The model structures for the same lattice constant (44.6 Å) are shown in Figures 1, 2, and 3 for wall thicknesses of 5.9, 8.4, and 10.9 Å, respectively. In previous simulations of glass surfaces using the same potential it was found that surface effects on the bond structure extend from the "flat" surface to at least 8 Å into the bulk. In view of this, the MCM-41 structures in the present model are dominated by surface effects. This interpretation is also supported by a ring distribution analysis. In the present discussion a ring of size N contains the *smallest* number of silicon

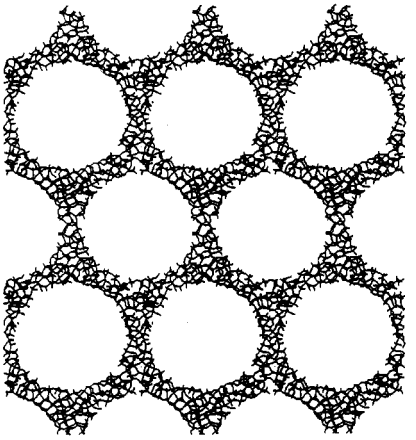

Figure 3. Model for MCM-41 with lattice constant of 44.6 Å and a wall thickness of 10.9 Å.

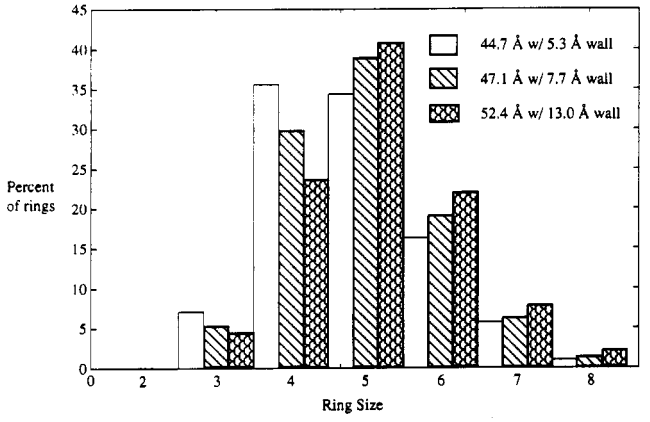

Figure 4. Ring distributions for the three models with the same micelle size and different lattice constants.

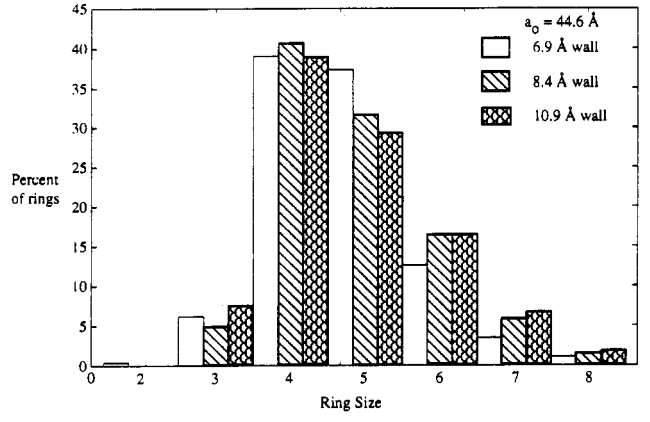

Figure 5. Ring distributions for the three models with the same lattice constant and different diameters for the micelles.

atoms (or N tetrahedra) necessary to complete a ring, where silicon neighbors in the ring are connected through a bridging oxygen. Six-membered rings are predominantly found in bulk amorphous silica, though three-membered rings are also expected to be present. The previous simulation of silica surfaces found a significant increase in the number of three- and four-membered rings near the surface.[7] The present analyses give similar results as seen in Figures 4 and 5. The ring distributions in Figure 4 refer to the models with the same micelle size while Figure 5 refers to the models with the same lattice constant. In contrast to bulk silica, all the present models have structures containing a majority of four- and five-membered rings. In Figure 4, the ring distributions show a clear trend toward larger rings with increasing wall thickness for fixed micelle size. However, the ring distribution for the structures with the same lattice spacing does not shift to larger ring sizes with increasing wall thicknesses, except for rings containing six or more tetrahedra.

TABLE 1: Comparison of Tetrahedral Site Density for Six Models of MCM-41[a]

model	lattice constant (Å)	pore radius (Å)	wall thickness (Å)	T-sites/1000 Å^3
1	44.7	19.7	5.3	7.9
2	47.1	19.7	7.7	9.1
3	52.4	19.7	13.0	11.6
4	44.6	19.4	5.9	6.8
5	44.6	18.1	8.4	8.8
6	44.6	17.9	10.9	11.0

[a] Models 1–3 have the same micelle size (pore radius) with various wall thicknesses, while models 4–6 have the same lattice constant (44.6 Å).

Two separate effects are competing when both the micelle size is reduced and the wall thickness is increased. From the results of the first three models, it is observed that increasing the wall thickness alone shifts the distribution of ring sizes to larger rings, similar to the distribution found in MD models for bulk silica. Small rings at the surface of silica are a result of reducing or eliminating dangling bonds that would be present at an arbitrary plane in the bulk material. As the wall thickness is increased for the same micelle, the surface-to-volume ratio decreases with a corresponding increase in the amount of bulklike silica. However, our results indicate that by reducing the micelle size, which increases the curvature of the oxygen-terminated silica surface, the layer of material which may be characterized as a surface extends further from the micelle–silica interface. In this case the distribution of rings shifts to smaller ring sizes. So the offsetting effects of decreasing micelle size and increasing wall thickness give rise to the rings distribution shown in Figure 5. From total energy considerations, i.e., surface atoms on average have a higher energy than bulk atoms, it is also apparent that the smaller micelles are generally less stable and therefore require thicker walls to achieve thermodynamic stability. Since these conclusions are based solely upon the bonding and topological defects of a silica surface, they are applicable only to MCM-41 with the organics removed.

In Table 1, pore size, wall thicknesses, and the density of T-sites are given for each of the model structures. Only the two structures (models 3 and 6), corresponding to the thickest walls, have T-site densities that fall in the zeolitic range of 11–18 T-sites per 1000 Å.[3] The concentration of silanols was also determined for each model structure by calculating the number of singly coordinated oxygen, i.e., nonbridging oxygen (NBO). These calculated values, ranging from 3.9/100 Å^2 to 8.4/100 Å^2, are in accord with the experimentally observed silanol concentrations of 4.5/100 Å^2 to 6.2/100 Å^2 for a vitreous silica (ν-SiO_2) surface.[10]

An X-ray diffraction pattern was calculated for each of the structures using the CERIUS Diffraction I software module.[11] Atomic coordinates and orthorhombic unit cell parameters were transferred to CERIUS from the MD simulation results. The atomic coordinates were obtained by averaging the positions of the final structures over a 10-ps MD run. The diffraction calculations used $P1$ space group symmetry, Cu Kα radiation, a conventional Lp correction, no temperature factors ($\beta = 0$), and appropriate powder multiplicities. Peak widths for the powder plots were calculated from the Scherrer equation using a 500-Å crystal size in the a, b, and c crystallographic directions. The calculated X-ray diffraction patterns show significant differences for the various lattice spacings and wall thicknesses as seen in Figures 6 and 7. These patterns are indexed on a hexagonal unit cell. Figure 6 shows the diffraction patterns for the three structures with the same micelle size while Figure 7 is for the structures with the same lattice spacing. As expected, the 100 peak uniformly shifts to smaller scattering angles with increasing lattice constant (Figure 6). The orthorhombic symmetry of the

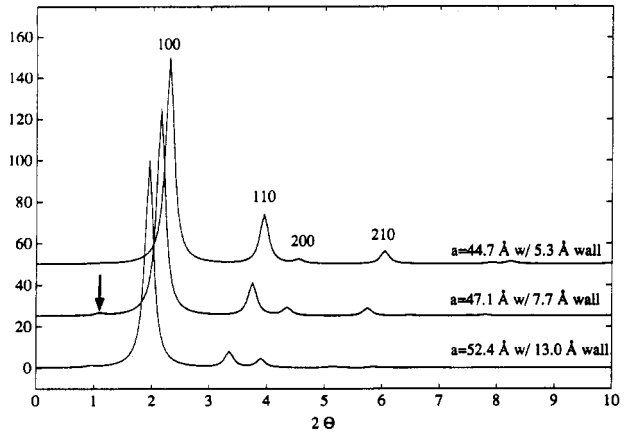

Figure 6. Simulated X-ray diffraction patterns for the three models with the same micelle size and different lattice constants. The arrow indicates a diffraction peak due to the periodicity of the molecular dynamics simulation cell.

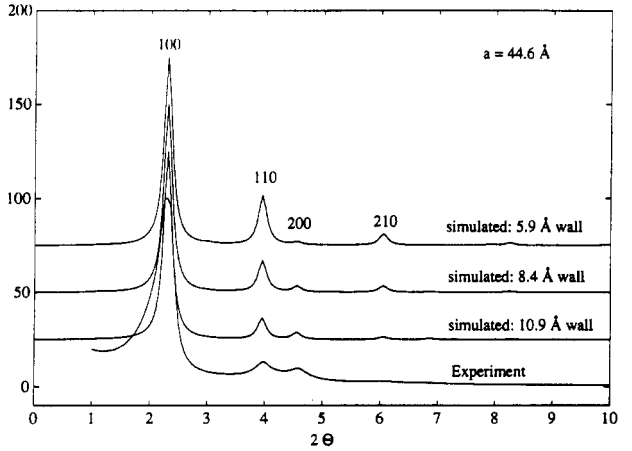

Figure 7. Simulated X-ray diffraction patterns for the three models with the same lattice constant and different diameters for the micelles. The X-ray diffraction results for a MCM-41 structure with the same lattice constant is shown for comparison.

MD cell appears only as a low diffraction peak as identified by the arrow in the middle pattern of Figure 6. The relative intensity of this diffraction peak was observed to decrease during the simulated annealing. Therefore, its presence in the calculated pattern is attributed to a system which is not quite fully relaxed but is not considered to be an important factor in the following discussion.

In both Figures 6 and 7, the 110 diffraction peak decreases in relative intensity with increasing wall thickness, with the 10.9- and 13.0-Å models in very good agreement with the experimentally observed diffraction pattern as seen in Figure 7 for the 10.9-Å wall. The relative intensity of the 210 peak to the 200 peak also shows a clear correlation with increasing wall thickness and is a good quantity to compare to the experiment. This ratio of intensities is much greater than 1.0 for the thin wall models, approximately equal to 1.0 for the structures with walls around 8 Å thick, and much less than 1.0 for the walls greater 11 Å. The latter is a signature of the observed X-ray diffraction pattern for all MCM-41 materials.

It is apparent that a large 110 diffraction peak is a signature of thin walls, though this may not be the only cause. The present investigation does not rule out the possibility that a narrow distribution of wall thicknesses may also yield a relatively large 110 diffraction peak. Phrased another way, a broad distribution of wall thicknesses may decrease the relative intensity of the 110 peak. Such a broad distribution around 8 Å may bring the corresponding X-ray diffraction pattern in better agreement with experiment.

Conclusions

A detailed atom-level description of the structure of the MCM-41 materials has been obtained. In particular, the relationship between wall thickness, micelle size, and observed X-ray diffraction pattern has been investigated. The diffraction pattern formed from amorphous silica with walls thicker than about 11 Å is in excellent agreement with experiment. Also, the densities of T-sites for these models fit within the known limits for large pore silicate frameworks. Silanol concentrations for all the structures simulated are in agreement with the values observed for vitreous silica surfaces. The percent of silicon which may be characterized by silanols are found to vary from 17% to 37%. A previous analysis of trimethylated MCM-41 by Si-NMR and of H-(MCM-41) by CRAMPS H-NMR found that only 8–27% of the silicons were silanols.[2] The model structures which are in agreement with the observed diffraction patterns have 17–28% of the silicons which are silanols in accord with the previous findings. In addition, the present results indicate that decreasing the diameter of the micelle template will lead to thicker walls between the hexagonally packed cylindrical pores.

Acknowledgment. We thank J. S. Beck, D. H. Olson, and J. H. Thurtell for valuable discussions concerning MCM-41 and the present model.

References and Notes

(1) Beck, J. S.; Vartuli, J. C.; Roth, W. J.; Leonowicz, M. E.; Kresge, C. T.; Schmitt, K. D.; Chu C. T.-W.; Olson, D. H.; Sheppard, E. W.; McCullen, S. B.; Higgins, J. B.; Schlenker, J. L. *J. Am. Chem. Soc.* **1992**, *114*, 10933.
(2) Chen, C. Y.; Li, H. X.; Davis, M. *Mesoporous Mater.* **1993**, *2*, 17.
(3) Woodcock, L. V.; Angell, C. A.; Cheeseman, P. *J. Chem. Phys.* **1976**, *65*, 1565.
(4) Sangster, M. J. L.; Dixon, M. *Adv. Phys.* **1976**, *25*, 247.
(5) Feuston, B. P.; Garofalini, S. H. *J. Chem. Phys.* **1988**, *89*, 5818.
(6) Newell, R. G.; Feuston, B. P.; Garofalini, S. H. *J. Mater. Res.* **1989**, *4*, 434.
(7) Feuston, B. P.; Garofalini, S. H. *J. Chem. Phys.* **1989**, *91*, 564.
(8) Feuston, B. P.; Garofalini, S. H. *Chem. Phys. Lett.* **1990**, *170*, 264.
(9) Feuston, B. P.; Garofalini, S. H. *J. Appl. Phys.* **1990**, *68*, 4830.
(10) Iler, R. K. *The Chemistry of Silica*; Wiley: New York, 1979.
(11) CERIUS, A Molecular modeling environment for materials research, distributed by Molecular Simulations, Inc., Cambridge, UK, 1991.